PHYSICAL REVIEW B **79**, 045205 (2009)

Spin-wave resonances and surface spin pinning in $Ga_{1-x}Mn_xAs$ thin films

C. Bihler,[1,*] W. Schoch,[2] W. Limmer,[2] S. T. B. Goennenwein,[3] and M. S. Brandt[1]
[1]*Walter Schottky Institut, Technische Universität München, Am Coulombwall 3, 85748 Garching, Germany*
[2]*Institut für Halbleiterphysik, Universität Ulm, 89069 Ulm, Germany*
[3]*Walther-Meissner-Institut, Bayerische Akademie der Wissenschaften, Walther-Meissner-Strasse 8, 85748 Garching, Germany*
(Received 1 December 2008; published 15 January 2009)

We investigate the dependence of the spin-wave resonance (SWR) spectra of $Ga_{0.95}Mn_{0.05}As$ thin films on the sample treatment. We find that for the external magnetic field perpendicular to the film plane, the SWR spectrum of the as-grown thin films and the changes upon etching and short-term hydrogenation can be quantitatively explained via a linear gradient in the uniaxial magnetic anisotropy field in growth direction. The model also qualitatively explains the SWR spectra observed for the in-plane easy-axis orientation of the external magnetic field. Furthermore, we observe a change in the effective surface spin pinning of the partially hydrogenated sample, which results from the tail in the hydrogen-diffusion profile. The latter leads to a rapidly changing hole concentration/magnetic anisotropy profile acting as a barrier for the spin-wave excitations. Therefore, short-term hydrogenation constitutes a simple method to efficiently manipulate the surface spin pinning.

DOI: 10.1103/PhysRevB.79.045205 PACS number(s): 75.50.Pp, 76.50.+g, 75.70.−i, 75.30.Ds

I. INTRODUCTION

Due to their particular magnetic and electronic properties and their promising application spectrum in spintronic devices, ferromagnetic semiconductors (FMS) are of continued scientific interest.[1–3] In $Ga_{1-x}Mn_xAs$, the most prominent representative of the class of III-V FMS, Mn substitution on the Ga lattice site both introduces the localized magnetic moment of the $3d^5$ electrons and acts as a relatively shallow acceptor. Even though it is well substantiated that the holes thus generated are mediating the ferromagnetic exchange interaction,[4] the details of this coupling—especially regarding the magnetization dynamics—are still under debate.[5]

The magnetic anisotropy of $Ga_{1-x}Mn_xAs$ thin films including the effects of strain, annealing, temperature, and doping has been investigated extensively especially via ferromagnetic resonance (FMR), with a review given in Ref. 6. While the special case of a spatially uniform precession of magnetization exists, in general, the precession amplitude varies as a function of position which in turn is described via spin-wave excitations (magnons) with nonzero wave vector k. In magnetic resonance selectively amplified spin-wave excitations fulfilling the boundary condition of the film can be detected, which we will refer to as spin-wave resonances (SWRs). The original Kittel model[7] for a homogeneous ferromagnetic thin film with pinned spins at the surfaces results in SWRs exhibiting a separation of successive SWR modes increasing proportionally to the mode index. However, for $Ga_{1-x}Mn_xAs$ thin films with thicknesses of a few 100 nm deviations from this Kittel mode-spacing behavior are generally reported.[8–13] These deviations have been attributed to the inhomogeneous magnetic properties of the $Ga_{1-x}Mn_xAs$ thin films as well as to the specific surface spin pinning conditions at the film surface and the film-substrate interface. In detail, a constant SWR spacing of successive modes for the external magnetic field oriented perpendicular to the film plane has been attributed to the presence of an effective uniaxial magnetic anisotropy field in the growth direction, varying quadratically with the distance from the film surface[11] or with the distance from the center of the film,[12,13] while a decreasing spacing has been attributed to a linear gradient in the anisotropy field with its maximum absolute value at the film surface.[9] Furthermore, also the surface spin pinning boundary conditions in $Ga_{1-x}Mn_xAs$ have been heavily debated in the context of SWR (Refs. 9 and 11–13) as well as light-induced magnetic precession[5] investigations.

So far the mode spacings and the relative mode intensities have always been explained via comparatively simple models for the uniaxial magnetic anisotropy profile and the surface spin pinning conditions. We here apply a more sophisticated analysis to this problem based on the discussion of the SWR spectra of inhomogeneous bubble garnet films by Hoekstra *et al.*[14] From the model for the anisotropy profile of $Ga_{1-x}Mn_xAs$ thin films developed here, we quantitatively derive the solutions of the spin-wave equation fulfilling the boundary condition of natural freedom. To investigate the validity of the conclusions drawn from the analysis of the as-grown thin film, we vary the thickness of the $Ga_{1-x}Mn_xAs$ layer by etching and we are able to straightforwardly account for the changes in the SWR spectrum observed.

An alternative approach to reduce the effective thickness of the ferromagnetic layer is hydrogenation. Postgrowth hydrogenation switches the ferromagnetic semiconductor $Ga_{1-x}Mn_xAs$ from ferromagnetic to a paramagnetic state via passivation of Mn acceptors.[15] A similar behavior upon hydrogenation has also been observed recently in $Ga_{1-x}Mn_xP$.[16] The incorporation of hydrogen induces a change in the effective oxidation state of the Mn atoms from +3 to +2, leading to a loss of holes mediating the magnetic order. Ferromagnetism and conductivity can be reactivated via posthydrogenation annealing.[16–19] It has been demonstrated that this annealing leads to a partial depassivation and thus enables an adjustment of the hole concentration as well as of the related ferromagnetic properties, in particular the Curie temperature and the magnetocrystalline anisotropy determining the orientations of the magnetic hard and easy

axes.[17,19,20] In this paper we take advantage of the property that hydrogenation suppresses the ferromagnetism as if the film would be removed by etching. The gradient in the hydrogen concentration—accompanied by a gradient in the hole concentration—resulting from the in diffusion of hydrogen leads to a region with varying uniaxial magnetic anisotropy field at the interface between the hydrogenated and the unhydrogenated parts of the sample. This region serves as a barrier for the spin-wave excitation and thus leads to an effective surface spin pinning which we will discuss in detail. We find that no such region is formed during wet-chemical etching, so that the spin waves remain free at the surface in the as-grown and etched samples.

II. EXPERIMENTAL DETAILS

$Ga_{1-x}Mn_xAs$ films with Mn concentrations $0.04<x<0.05$ and thicknesses $100<d<330$ nm were grown via low-temperature molecular-beam epitaxy (LTMBE) on In-mounted (001)-oriented semi-insulating GaAs substrates.[21] The FMR measurements were performed with a Bruker ESP 300 electron-paramagnetic-resonance spectrometer with a TE_{102} cavity at a constant microwave frequency of $\omega/2\pi \approx 9.3$ GHz, with the sample temperature adjusted to 5 K using a liquid-He flow cryostat. For lock-in detection we apply magnetic field modulation with amplitude of $\mu_0 H_{\mathrm{mod}} = 3.2$ mT and frequency of $f_{\mathrm{mod}} = 100$ kHz. We generally find that samples that were grown at a low V/III flux ratio[22] exhibit several SWR excitations with a decreasing separation of successive SWR modes with increasing mode number. In most samples the SWR pattern could be well described via a linear gradient in the uniaxial anisotropy field in growth direction as discussed in Ref. 9. Nonetheless, in some samples the decreasing behavior of mode separation with mode number was less pronounced. Note that a constant mode separation would correspond to a parabolic gradient as described by Rappoport *et al.*[11] Since most samples exhibiting SWR modes showed a similar spacing and also similar relative intensities of the modes, we here exemplarily focus in a very detailed analysis on one representative $Ga_{1-x}Mn_xAs$ thin film with a Mn concentration of $x=0.05$ and a film thickness of 175 nm derived from high-resolution x-ray diffraction (HRXRD).

Figure 1 shows the FMR spectra of several pieces of the same film etched to different thicknesses in a 38:1:1 by volume solution of water, hydrogen peroxide, and phosphoric acid with the external magnetic field oriented perpendicular to the film plane at 5 K. Due to lock-in detection and accompanied magnetic field modulation, each resonance is represented by the derivative of a microwave absorption line. As already reported earlier[9] the maximum observed resonance field decreases linearly as a function of the etching depth determined via a Dektak profilometer. Note that for an etch depth of 130 nm—which is still well below the geometrical sample thickness—no FMR could be observed anymore. Thus we conclude that at least for the sample under consideration, the ferromagnetic film thickness is smaller than the geometric film thickness. As we will show below, this finding is in perfect agreement with our simulations of the SWR

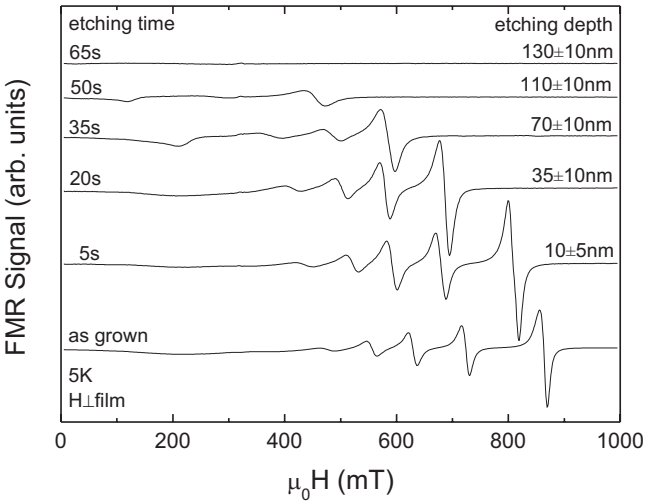

FIG. 1. FMR spectra at 5 K with the external magnetic field oriented perpendicular to the film plane of $Ga_{0.95}Mn_{0.05}As$ thin films etched to different thicknesses in a 38:1:1 by volume solution of H_2O, H_2O_2, and H_3PO_4. For clarity, the individual spectra are shifted vertically.

spectra. For comparison with the etched samples we subjected another piece of sample to partial hydrogenation for 2 h via a remote direct current (dc) hydrogen plasma operated at 0.9 mbar with the sample heated to 170 °C.[15,16]

III. SWR THEORY

The time-dependent evolution of the magnetization orientation is described via the Landau-Lifshitz-Gilbert equation,[23,24]

$$\frac{\partial \vec{M}}{\partial t} = -\gamma \vec{M} \times (\mu_0 \vec{H}_{\mathrm{eff}}) + \frac{\tilde{G}}{\gamma M_{\mathrm{sat}}^2} \vec{M} \times \frac{\partial \vec{M}}{\partial t}, \tag{1}$$

with the time t, the gyromagnetic ratio $\gamma = g\mu_B/\hbar$, the g factor g, the Bohr magneton μ_B, the reduced Planck constant $\hbar$, the magnetization $\vec{M}$, the saturation magnetization M_{sat}, the vacuum permeability μ_0, the effective magnetic field within the ferromagnetic layer $\vec{H}_{\mathrm{eff}}$, and the Gilbert damping parameter $\tilde{G}$, which is also often taken into account via the dimensionless phenomenological damping parameter[25] $\alpha = \tilde{G}/(\gamma M_{\mathrm{sat}})$. In the following we will focus especially on the first term on the right-hand side of Eq. (1) and neglect the damping term, which determines the linewidth of the resonance. The effective field $\vec{H}_{\mathrm{eff}}$ in the first term is given by

$$\vec{H}_{\mathrm{eff}} = \vec{H} + \vec{H}_{\mathrm{aniso}}^{\vec{e}_M} + \frac{D}{\mu_0 M_{\mathrm{sat}}} \nabla^2 \vec{M} + \vec{h}_{\mathrm{rf}}, \tag{2}$$

where $\vec{H}$ is the external magnetic field, $D = 2A/M_{\mathrm{sat}}$ is the exchange constant with the exchange stiffness A, and $\vec{h}_{\mathrm{rf}}$ is the driving radio-frequency (rf) field of the microwave. The anisotropy field $\vec{H}_{\mathrm{aniso}}^{\vec{e}_M}$, in general, is a function of the magnetization orientation $\vec{e}_M = \vec{M}/M_{\mathrm{sat}} = (\alpha_x, \alpha_y, \alpha_z)$ with the di-

rection cosines α_i of $\vec{e}_M$ along the Cartesian axes, $i \in \{x,y,z\}$. It can be derived from the free-energy volume density,

$$F = -K_{\text{eff}}^{001}\alpha_z^2 - \frac{1}{2}K_{c1}^{\perp}\alpha_z^4 - \frac{1}{2}K_{c1}^{\parallel}(\alpha_x^4 + \alpha_y^4) \tag{3}$$

via[26,44,45]

$$\mu_0 \vec{H}_{\text{aniso}}^{\vec{e}_M} = -\frac{1}{M_{\text{sat}}}\nabla_{\vec{e}_M} F, \tag{4}$$

where $\nabla_{\vec{e}_M} = (\partial_{\alpha_x}, \partial_{\alpha_y}, \partial_{\alpha_z})$ is the vector differential operator with respect to the components of the unit vector $\vec{e}_M$. The effective uniaxial anisotropy parameter in the growth direction $K_{\text{eff}}^{001} = K_u^{001} - \frac{1}{2}\mu_0 M_{\text{sat}}^2$ is composed of the uniaxial magnetocrystalline component K_u^{001} and the demagnetization contribution $\frac{1}{2}\mu_0 M_{\text{sat}}^2$. The origin of K_u^{001} is the compressive epitaxial strain of the $Ga_{1-x}Mn_xAs$ layer grown pseudomorphically on the GaAs substrate.[27–29] $K_{c1}^{\perp}$ and $K_{c1}^{\parallel}$ are the cubic anisotropy parameters in growth direction and within the film plane, respectively, which may differ due to the epitaxial strain. Via Eq. (4) the anisotropy field as a function of magnetization orientation $\vec{e}_M$ thus can be derived to

$$\mu_0 \vec{H}_{\text{aniso}}^{\vec{e}_M} = \frac{2K_{c1}^{\parallel}}{M_{\text{sat}}}(\alpha_x^3 \vec{e}_x + \alpha_y^3 \vec{e}_y) + \left(\frac{2K_{\text{eff}}^{001}}{M_{\text{sat}}}\alpha_z + \frac{2K_{c1}^{\perp}}{M_{\text{sat}}}\alpha_z^3\right)\vec{e}_z, \tag{5}$$

where $\vec{e}_i$, $i \in \{x,y,z\}$, denote the unit vectors along the Cartesian axes.

In the following we will consider the special case of the external magnetic field $\vec{H} = H\vec{e}_z$ aligned along the z direction. At sufficiently large magnetic fields—a condition that is fulfilled in our SWR experiments—the magnetization will also be aligned along the $\vec{e}_z$ direction, i.e., $\vec{e}_M = (0,0,1)$, resulting in $\mu_0 \vec{H}_{\text{aniso}}^{001} = 2(K_{\text{eff}}^{001} + K_{c1}^{\perp})/M_{\text{sat}}\vec{e}_z$.

Further on, we assume a variation in the magnetic properties only along the growth direction, i.e., z direction. Especially, we take into account an inhomogeneous anisotropy field $\vec{H}_{\text{aniso}}^{001}(z) = H_{\text{aniso}}^{001}(z)\vec{e}_z$. Therefore, the $\vec{h}_{\text{rf}}$-induced excitations of the magnetic moments can be described via $\vec{M}(z) = M_z\vec{e}_z + \tilde{m}(z)e^{-i\omega t}(\vec{e}_x + i\vec{e}_y)$, with a z-dependent rf magnetization $\tilde{m} \ll M_{\text{sat}}$ within the film plane and $M_z \approx M_{\text{sat}}$. Putting this expression for $\vec{M}(z)$ into Eq. (1) and neglecting the damping term, we obtain the spin-wave equation,

$$D\partial_z^2 \tilde{m}(z) + \left[-\mu_0 H - \mu_0 H_{\text{aniso}}^{001}(z) + \frac{\omega}{\gamma}\right]\tilde{m}(z) = 0, \tag{6}$$

which has the form of the one-dimensional time-independent Schrödinger equation of a particle with wave function $\psi(z)$ and mass m_0 in a potential $V(z)$,

$$\frac{\hbar^2}{2m_0}\partial_z^2 \psi(z) + [E - V(z)]\psi(z) = 0, \tag{7}$$

where $\tilde{m}(z)$ corresponds to $\psi(z)$, D to $\hbar^2/2m_0$, $-\mu_0 H$ to the energy E, and $\mu_0 H_{\text{aniso}}^{001}(z) - \omega/\gamma$ to $V(z)$.[14,30,31] Consequently, the resonance fields $H_{\text{res},n}$ (=eigenvalues) and the corresponding spin-wave profile $\tilde{m}_n(z)$ (=eigenvectors) for a given profile of the so-called uniform resonance

$$\mu_0 H_{\text{un}}^{001}(z) = \omega/\gamma - \mu_0 H_{\text{aniso}}^{001}(z) \tag{8}$$

can be determined via solving

$$D\partial_z^2 \tilde{m}(z) + [-\mu_0 H + \mu_0 H_{\text{un}}^{001}(z)]\tilde{m}(z) = 0 \tag{9}$$

in the same way as the energy eigenvalues E_n, and the corresponding wave functions $\psi_n(z)$ can be determined via solving Eq. (7) for a given potential profile $V(z)$. The meaning of the uniform resonance profile can be visualized as follows. A homogeneous film with a constant anisotropy field $\mu_0 H_{\text{aniso}}^{001}$ throughout the layer exhibits a single so-called uniform resonance at $\mu_0 H_{\text{un}}^{001}$ for $\vec{H}$ perpendicular to the film plane, which corresponds to an excitation of the magnetic moments described by a constant $\tilde{m}_n(z) = \tilde{m}_0$ throughout the layer. If the ferromagnetic film would consist of a sequence of uncoupled ferromagnetic layers with varying $\mu_0 H_{\text{aniso}}^{001}(z)$, each layer would be in resonance at a different external magnetic field $\mu_0 H_{\text{un}}^{001}(z)$. Due to the exchange coupling of the magnetic moments in neighboring magnetic layers described by D, the uniform resonance is no longer a solution of the resonance Eq. (6), but the solution $\tilde{m}_n(z)$ has to be derived via the formalism described in Sec. V.

As discussed in detail in Ref. 32, a spin-wave excitation can be described in second quantization via creation and annihilation Bose operators, resulting in the orthonormality of the eigenvectors $\tilde{m}_n(z)$. The intensity I_n with which an individual spin wave $\tilde{m}_n(z)$ is excited in a SWR experiment can be derived from Fermi's golden rule to[32,33]

$$I_n \propto \frac{\left|\int_0^L \tilde{m}_n(z)dz\right|^2}{\int_0^L |\tilde{m}_n(z)|^2 dz}, \tag{10}$$

where $z=0$ corresponds to the film surface and $z=L$ corresponds to the film-substrate interface.

IV. SURFACE SPIN PINNING CONDITIONS

The pinning conditions of the spin wave correspond to the boundary conditions imposed on the $\tilde{m}_n(z)$. In the original Puszkarski surface inhomogeneity model[32] the ferromagnetic thin film is composed of a sequence of layers of magnetic moments each arranged in the (001) plane. Within each layer the magnetic moments are aligned parallel and the spin wave is formed by a continuous tilt of the magnetization orientation between neighboring layers along the $\vec{e}_z$ direction. Surface spin pinning is caused by an effective surface anisotropy field $\vec{K}_{\text{surf}}^{\text{Pus}}$, which in the Puszkarski model (Pus) is present exclusively in the two surface layers—i.e., the two layers at the film surface and the film-substrate interface. Note that in the following we use a slightly deviating definition for the surface anisotropy field,[31]

$$\frac{2\vec{K}_{\mathrm{surf}}}{M_{\mathrm{sat}}} = a\vec{K}^{\mathrm{Pus}}_{\mathrm{surf}}, \tag{11}$$

where a denotes the separation between the neighboring layers of magnetic moments. According to Puszkarski[32] the pinning can be described by the surface parameter A^* which is connected with $\vec{K}_{\mathrm{surf}}$ via[34]

$$A^* = 1 - \frac{g\mu_B}{S\zeta aJM^2_{\mathrm{sat}}}\vec{M}\cdot\vec{K}_{\mathrm{surf}}, \tag{12}$$

where ζ denotes the number of nearest-neighbor magnetic moments with spin S in neighboring layers and J denotes the Heisenberg exchange integral between them. For $\vec{M}=M_{\mathrm{sat}}\vec{e}_z$ and $\vec{K}_{\mathrm{surf}}=K_{\mathrm{surf}}\vec{e}_z$ the pinning is given by

$$(\partial_z\tilde{m})/\tilde{m} = \pm\frac{2K_{\mathrm{surf}}}{M_{\mathrm{sat}}}\Big/D, \tag{13}$$

where the "+" sign applies to the film surface and the "–" sign applies to the film-substrate interface.[31,35,36] Two general cases can be distinguished. For $A^*<1$ ($K_{\mathrm{surf}}>0$) the spins are pinned, while for $A^*>1$ ($K_{\mathrm{surf}}<0$) the spins are unpinned. In addition, there are several special cases. For $A^*=1$ ($K_{\mathrm{surf}}=0$) the surface spins exhibit *natural freedom*. This corresponds to the natural pinning condition of a surface, which only takes into account the fact that due to the reduced number of nearest neighbors, the spins at the surface are freer than the internal spins within the film. In this case $\partial_z\tilde{m}=0$ has to be fulfilled at the surface. For $A^*=0$ the natural freedom of the surface spins is compensated and their pinning becomes equal to internal spins.[31] Finally, for $A^*=+\infty$ and $-\infty$ there is perfect freedom and perfect pinning, respectively. In the following we will demonstrate that for the description of our experiments it is sufficient to generally assume natural freedom, i.e., $\partial_z\tilde{m}=0$ at both the surface of the $Ga_{1-x}Mn_xAs$ layer and at the interface to the substrate.

V. SWR SIMULATION

To simulate our SWR measurements we subdivide the ferromagnetic layer into four regions [compare Fig. 2(a)]. (0) $0<z<z_0$: this region accounts for a reduction in the thickness of the ferromagnetic layer by z_0 via etching or complete passivation. Consequently, $z=0$ denotes the surface of the as-grown layer and $z=z_0$ denotes the surface of the ferromagnetic layer in the case where its thickness is reduced upon postgrowth treatment. (I) $z_0<z<z_{\mathrm{I}}$: in the case of the partially hydrogenated sample our model includes at the surface of the ferromagnetic layer this region of thickness $L_{\mathrm{I}}=z_{\mathrm{I}}-z_0$ with constant $H^{001}_{\mathrm{aniso}}(z)=H^{001}_{\mathrm{aniso,I}}$, which accounts for the strongly inhomogeneous hydrogenation profile. Note that Fig. 2(a) shows the profile of the so-called uniform resonance $\mu_0H^{001}_{\mathrm{un}}(z)$ introduced in Eq. (8). The corresponding profile of the anisotropy field is given by $\mu_0H^{001}_{\mathrm{aniso}}(z)=\omega/\gamma-\mu_0H^{001}_{\mathrm{un}}(z)$. (II) $z_{\mathrm{I}}<z<z_{\mathrm{II}}$: the corpus of the ferromagnetic layer is described by a region of thickness $L_{\mathrm{II}}=z_{\mathrm{II}}-z_{\mathrm{I}}$, exhibiting a linear gradient in $\mu_0H^{001}_{\mathrm{aniso}}(z)=G(z-z_{\mathrm{I}})+C$ with slope G. (III) $z_{\mathrm{II}}<z<z_{\mathrm{III}}=L$: finally there is a region of thickness

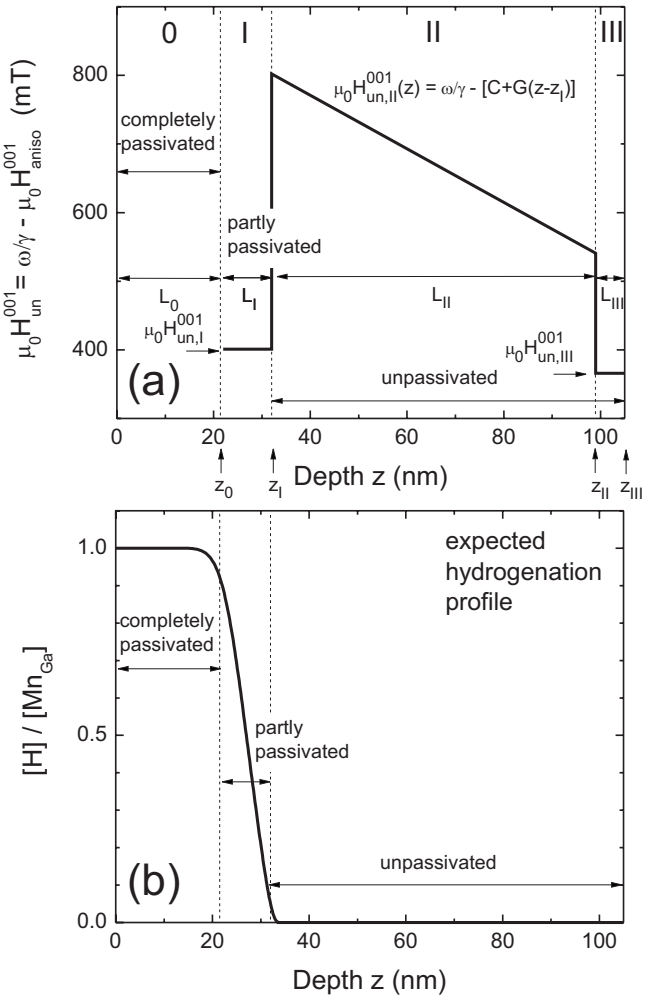

FIG. 2. (a) Uniform resonance field profile $\mu_0H^{001}_{\mathrm{un}}(z)$ used for the simulation of the SWR spectrum of the partially hydrogenated sample. The profile is subdivided into several regions: (0) $0<z<z_0$, fully passivated, ferromagnetism suppressed; (i) $z_0<z<z_{\mathrm{I}}$, partially passivated, $\mu_0H^{001}_{\mathrm{un}}(z)=\mu_0H^{001}_{\mathrm{un,I}}$, (II) $z_{\mathrm{I}}<z<z_{\mathrm{II}}$, linear gradient $\mu_0H^{001}_{\mathrm{un}}(z)=\omega/\gamma-[G(z-z_{\mathrm{I}})+C]$; and (III) $z_{\mathrm{II}}<z<z_{\mathrm{III}}$, $\mu_0H^{001}_{\mathrm{un}}(z)=\mu_0H^{001}_{\mathrm{un,III}}$. In the case of an etched sample the thickness of region 0 corresponds to the etch depth and the thickness of region I, $L_{\mathrm{I}}=0$. (b) Schematic hydrogenation profile used to account for the profile of the uniform resonance field in (a).

$L_{\mathrm{III}}=z_{\mathrm{III}}-z_{\mathrm{II}}$ with constant $H^{001}_{\mathrm{aniso}}(z)=H^{001}_{\mathrm{aniso,III}}$, which describes the magnetic properties of the ferromagnetic layer in the vicinity of the interface to the substrate.

In regions I and III the solution of Eq. (6) results in a spin-wave profile described by[31]

$$\tilde{m}_{n,\mathrm{I}}(z) = a\cos(k_{n,\mathrm{I}}z) + b\sin(k_{n,\mathrm{I}}z) \tag{14}$$

and

$$\tilde{m}_{n,\mathrm{III}}(z) = e\cos(k_{n,\mathrm{III}}z) + f\sin(k_{n,\mathrm{III}}z), \tag{15}$$

respectively. Here $k_{n,i}$ denotes the effective wave vector in region i which is given by[37]

$$k_{n,i}^2 = \frac{1}{D}\left(-\mu_0 H_{\mathrm{res},n} - \mu_0 H_{\mathrm{aniso},i}^{001} + \frac{\omega}{\gamma}\right) \tag{16}$$

for $i \in \{\mathrm{I}, \mathrm{III}\}$. Substituting

$$x = \frac{1}{l}\left[(z - z_{\mathrm{I}}) + \frac{1}{G}\left(\mu_0 H + C - \frac{\omega}{\gamma}\right)\right] \tag{17}$$

with the characteristic length

$$l = \left(\frac{D}{G}\right)^{1/3} \tag{18}$$

in region II, Eq. (6) transforms into[14,31]

$$\partial_x^2 \tilde{m}(x) - x\tilde{m}(x) = 0. \tag{19}$$

Consequently, the solution of Eq. (6) in region II is given by

$$\tilde{m}_{n,\mathrm{II}}(z) = c\ \mathrm{Ai}[-l^2 k_{n,\mathrm{II}}^2(z)] + d\ \mathrm{Bi}[-l^2 k_{n,\mathrm{II}}^2(z)], \tag{20}$$

with the Airy functions $\mathrm{Ai}(x)$ and $\mathrm{Bi}(x)$, which exhibit oscillatory behavior for $x<0$. For $x>0$, $\mathrm{Ai}(x)$ $[\mathrm{Bi}(x)]$ exponentially decreases (increases). Note that the effective wave vector $k_{n,\mathrm{II}}$ in region II exhibits a z dependence,

$$k_{n,\mathrm{II}}^2(z) = \frac{1}{D}\left\{-\mu_0 H_{\mathrm{res},n} - [G(z - z_{\mathrm{I}}) + C] + \frac{\omega}{\gamma}\right\}. \tag{21}$$

The parameters a, b, c, d, e, and f can be derived from the boundary conditions imposed by the assumption of natural freedom $\partial_z \tilde{m}_{n,\mathrm{I}}(z)|_{z=z_0}=0$ and $\partial_z \tilde{m}_{n,\mathrm{III}}(z)|_{z=L}=0$, as well as the continuity conditions $\tilde{m}_{n,\mathrm{I}}(z_{\mathrm{I}})=\tilde{m}_{n,\mathrm{II}}(z_{\mathrm{I}})$, $\partial_z \tilde{m}_{n,\mathrm{I}}(z)|_{z=z_{\mathrm{I}}} = \partial_z \tilde{m}_{n,\mathrm{II}}(z)|_{z=z_{\mathrm{I}}}$, $\tilde{m}_{n,\mathrm{II}}(z_{\mathrm{II}})=\tilde{m}_{n,\mathrm{III}}(z_{\mathrm{II}})$, and $\partial_z \tilde{m}_{n,\mathrm{II}}(z)|_{z=z_{\mathrm{II}}} = \partial_z \tilde{m}_{n,\mathrm{III}}(z)|_{z=z_{\mathrm{II}}}$. Finally the spin wave has to be normalized according to

$$\int_0^L |\tilde{m}_n(z)|^2 dz = 1. \tag{22}$$

This results in a set of curves A_n fulfilling these boundary conditions, characterized by the different number of nodes $n-1$ of the corresponding spin wave $\tilde{m}_n(z)$. Each curve A_n is given by a list of $\{l^2 k_{n,\mathrm{II}}^2(z_{\mathrm{I}}), l^2 k_{n,\mathrm{II}}^2(z_{\mathrm{II}})\}$. The gradient in $H_{\mathrm{aniso}}^{001}(z)$ imposes an additional restriction on the effective wave vectors at the boundaries of region II,

$$l^2 k_{n,\mathrm{II}}^2(z_{\mathrm{I}}) = l^2 k_{n,\mathrm{II}}^2(z_{\mathrm{II}}) \pm \frac{L_{\mathrm{II}}}{l}, \tag{23}$$

where the sign of the last term is + for $G>0$ (Fig. 3) and − for $G<0$ (Fig. 4).

In the following we will apply this model to simulate the SWR spectra of the as-grown sample, the sample etched for 20 s, and the partially hydrogenated sample. Furthermore, we will show that the change in surface spin pinning observed upon partial hydrogenation can be explained by the presence of a surface layer (I) which corresponds to a region with strongly inhomogeneous hydrogenation profile. The latter induces a $\mu_0 H_{\mathrm{aniso}}^{001}(z)$ profile, which is strongly inhomogeneous on a length scale below the characteristic length l and thus can be described by an average constant $\mu_0 H_{\mathrm{aniso}}^{001}(z) = \mu_0 H_{\mathrm{aniso,I}}^{001} = \omega/\gamma - \mu_0 H_{\mathrm{un,I}}^{001}$.

VI. AS-GROWN SAMPLE

Figure 3(a) shows the SWR spectrum measured in the as-grown sample at 5 K for the external magnetic field oriented perpendicular to the sample plane. The spectrum in Fig. 3(a) exhibits at least six spin-wave resonance excitations of continuously decreasing intensity and decreasing spacing labeled with a running index $n=1,2,\ldots,6$. A similar spectrum has already been traced back to the presence of a linear gradient in $H_{\mathrm{aniso}}^{001}(z)$.[9] Here we quantitatively reproduce the spectrum via the model derived in Secs. III–V. For the as-grown sample [i.e., the SWR in Fig. 3(a)] we use $L_{\mathrm{I}}=0$, $L_{\mathrm{II}}=99$ nm, $L_{\mathrm{III}}=6$ nm, $G=3.9$ mT/nm, $C=-597$ mT, $\mu_0 H_{\mathrm{aniso,III}}^{001}=-211$ mT, $D=16$ Tnm^2, and $l=16.0$ nm.

For the $\mu_0 H_{\mathrm{un}}^{001}(z)$ profile shown in Fig. 3(c), the pairs of effective wave vectors $\{l^2 k_{n,\mathrm{II}}^2(z_{\mathrm{I}}), l^2 k_{n,\mathrm{II}}^2(z_{\mathrm{II}})\}$ fulfilling the boundary condition of natural freedom for a different number of nodes $(n-1)$ are given by the curves A_n in Fig. 3(b). Furthermore, the straight diagonal line represents the restriction additionally imposed by Eq. (23). Thus the solutions $\{l^2 k_{n,\mathrm{II}}^2(z_{\mathrm{I}}), l^2 k_{n,\mathrm{II}}^2(z_{\mathrm{II}})\}$ fulfilling both restrictions are obtained from the intersection points labeled with n. Figure 3(c) displays the corresponding spin-wave excitations $\tilde{m}_n(z)$ plotted at their respective resonance field $\mu_0 H_{\mathrm{res},n}$. The $\mu_0 H_{\mathrm{res},n}$ are derived via insertion of $k_{n,\mathrm{II}}(z_{\mathrm{I}})$ into Eq. (21). For each position z the effective wave vector is given by

$$k_n(z) = \sqrt{\frac{1}{D}[\mu_0 H_{\mathrm{un}}^{001}(z) - \mu_0 H_{\mathrm{res},n}]}. \tag{24}$$

Hence, as long as $\mu_0 H_{\mathrm{un}}^{001}(z) > \mu_0 H_{\mathrm{res},n}$, $k_n(z)$ is real and $\tilde{m}_n(z)$ exhibits oscillatory behavior, while for $\mu_0 H_{\mathrm{un}}^{001}(z) < \mu_0 H_{\mathrm{res},n}$, $k_n(z)$ becomes imaginary and $\tilde{m}_n(z)$ consequently decreases exponentially. A localization of the modes in the vicinity of the film surface together with an exponential decrease toward the film-substrate interface can be observed for $n=1-3$, while for $n\geq 4$ the oscillatory behavior of $\tilde{m}_n(z)$ extends over the complete thickness of the ferromagnetic film and the corresponding modes thus can be considered as volume modes. The dashed curve in Fig. 3(a) represents the SWR spectrum calculated from a superposition of the derivatives of Lorentzian curves at resonance positions $\mu_0 H_{\mathrm{res},n}$ multiplied by the respective intensities I_n calculated from Eq. (10) and a peak-to-peak linewidth of $\mu_0 \Delta H_{\mathrm{p.p.}}=14$ mT. Both the resonance positions and the relative intensities are well reproduced by our simulation. Note that the maximum observed resonance field $\mu_0 H_{\mathrm{res},1}=863$ mT is $\delta=64$ mT smaller than the uniform resonance field at the surface of the film $\mu_0 H_{\mathrm{un}}^{001}(0)=927$ mT derived from our SWR simulation. Therefore, care should be taken at the extraction of anisotropy fields from an anisotropic SWR pattern since the assumption that the resonance field of the first SWR corresponds to the field of the uniform resonance often is not justified.[13]

We attribute the gradient in the magnetic properties to the presence of a gradient in hole concentration p. Electrochemical capacitance voltage (ECV) profiling and Raman spectroscopy in $Ga_{1-x}Mn_xAs$ thin films similar to the one studied here have shown that p monotonically decreases from its

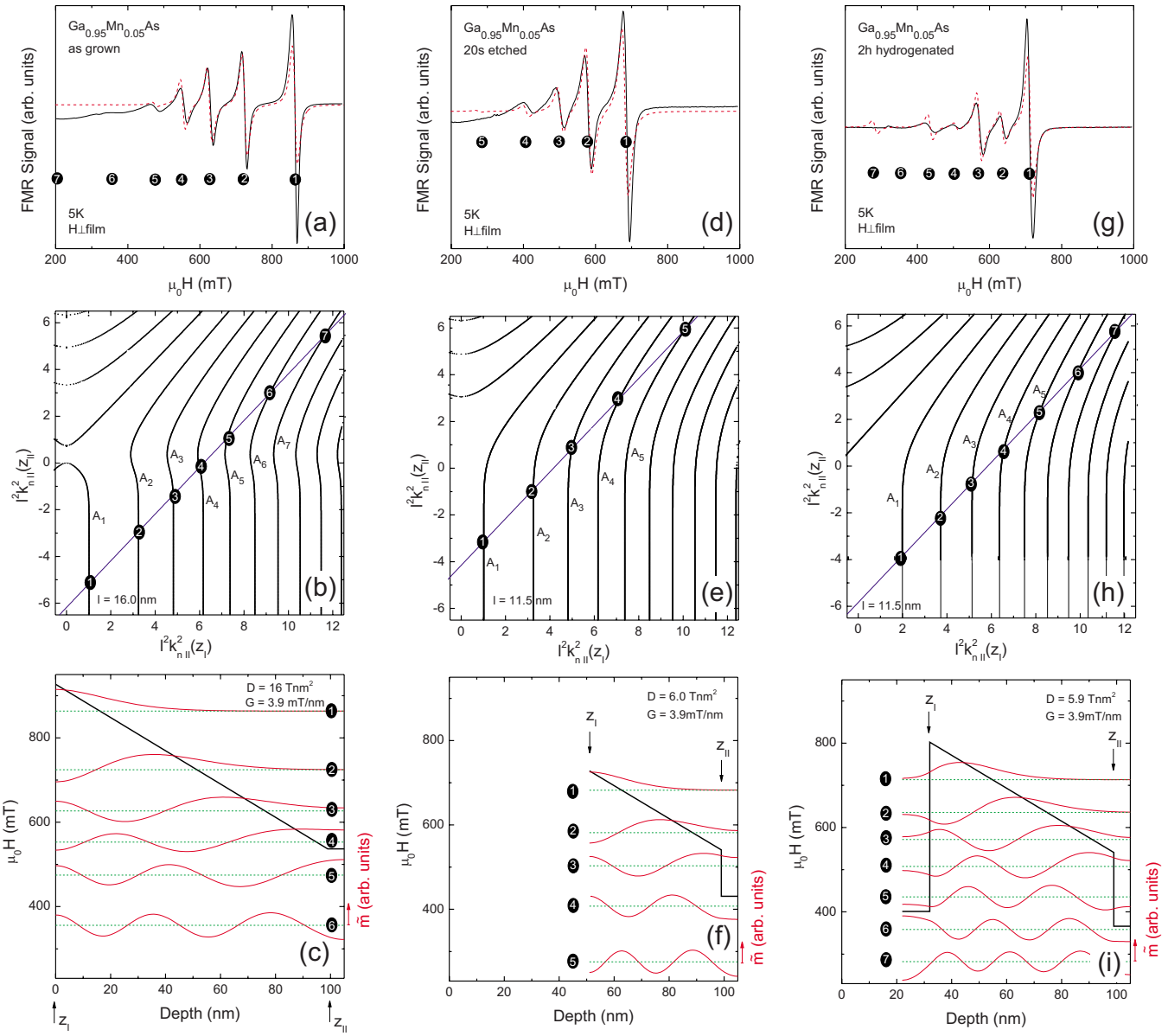

FIG. 3. (Color online) Experimental (full curves) and simulated (dashed curves) SWR spectra for $\vec{H}\|[001]$ perpendicular to the film plane of (a) the as-grown, (d) the etched, and (g) the partially hydrogenated samples. In (b), (e), and (h) the pairs of effective wave vectors $\{l^2k^2_{n,\mathrm{II}}(z_\mathrm{I}), l^2k^2_{n,\mathrm{II}}(z_\mathrm{II})\}$ fulfilling the boundary condition of natural freedom for the $\mu_0 H^{001}_{\mathrm{un}}(z)$ profiles displayed as thick solid black lines in (c), (f), and (i), respectively, are represented by the set of curves A_n. The straight diagonal line in (b), (e), and (h) represents restriction (23) additionally imposed by the linear gradient in $H^{001}_{\mathrm{aniso}}(z)$. From the intersection points the solutions of the spin wave equation [Eq. (6)] are derived with the spin-wave excitations $\tilde{m}_n(z)$ plotted at the positions of the corresponding resonance field $\mu_0 H_{\mathrm{res},n}$ indicated by thin dashed lines in (c), (f), and (i).

maximum value near the sample surface to the $Ga_{1-x}Mn_xAs/GaAs$ interface.[38,39] This could be due to diffusion and/or rearrangement of Mn interstitials[40,41] during and just after the growth with the sample still loaded in the MBE chamber.

VII. ETCHED SAMPLE

Due to the linear gradient in $\mu_0 H^{001}_{\mathrm{aniso}}(z)$ in the as-grown $Ga_{1-x}Mn_xAs$ film, a reduction in the thickness of the ferromagnetic layer via etching will lead to a reduction in $\mu_0 H^{001}_{\mathrm{un}}$ at the surface of the film [Figs. 3(c) and 3(f)]. Therefore, also the spin-wave excitations $\mu_0 H_{\mathrm{res},n}$ are expected to follow this shift to smaller magnetic fields, which indeed is observed in the SWR spectrum of the etched samples [Figs. 1 and 3(d)]. Furthermore, the spin-wave excitations still monotonically decrease in intensity I_n with increasing mode index n. In the following we discuss the simulation of the SWR spectrum of the sample etched for 20 s by an etch depth of 35 ± 10 nm (Fig. 1). The dashed curve in Fig. 3(d) represents the result

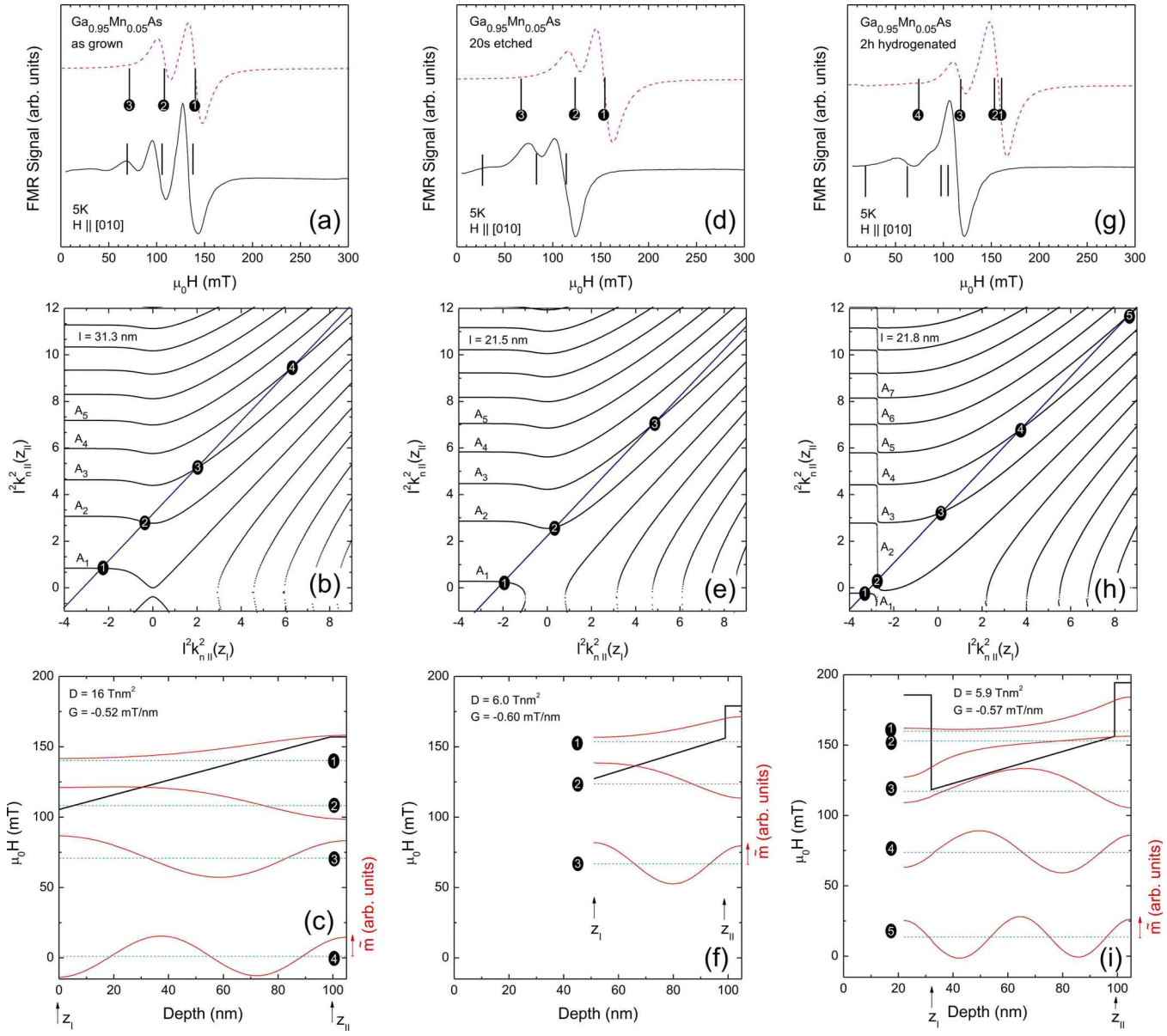

FIG. 4. (Color online) Experimental (full curves) and simulated (dashed curves) SWR spectra for $\vec{H}\|[010]$ within the film plane of (a) the as-grown, (d) the etched, and (g) the partially hydrogenated samples. The straight vertical lines point out the SWR spacing of the simulated spectra. For better comparison with the experimental data they are also shown shifted horizontally. In (b), (e), and (h) the pairs of effective wave vectors $\{l^2k^2_{n,\mathrm{II}}(z_\mathrm{I}), l^2k^2_{n,\mathrm{II}}(z_\mathrm{II})\}$ fulfilling the boundary condition of natural freedom for the $\mu_0 H^{001}_{\mathrm{un}}(z)$ profiles displayed as thick solid black lines in (c), (f), and (i), respectively, are represented by the set of curves A_n. The straight vertical line in (b), (e), and (h) represents restriction (23) additionally imposed by the linear gradient in $H^{001}_{\mathrm{aniso}}(z)$. From the intersection points the solutions of the spin wave equation [Eq. (28)] are derived with the spin-wave excitations $\tilde{m}_n(z)$ plotted at the positions of the corresponding resonance field $\mu_0 H_{\mathrm{res},n}$ indicated by thin dashed lines in (c), (f), and (i).

of a simulation [Figs. 3(e) and 3(f)] with $L_\mathrm{I}=0$, $L_\mathrm{II}=48$ nm, $L_\mathrm{III}=6$ nm, $G=3.9$ mT/nm, $C=-398$ mT, $\mu_0 H^{001}_{\mathrm{aniso,III}}=-101$ mT, $D=6$ T nm^2, $l=11.5$ nm, and $\mu_0\Delta H_{\mathrm{p.p.}}=17$ mT. The reduction in both L_II and C accounts for the reduction in the thickness of the ferromagnetic layer by 51 nm upon etching, which is in reasonable agreement with the etch depth of 35 ± 10 nm determined via mechanical profilometry. In our simulation we assume a constant exchange parameter D throughout the ferromagnetic layer. Since the etched sample exhibits a significantly reduced D compared to the as-grown one, this assumption has to be regarded as an approximation. Also, the fact that we have to assume a different $\mu_0 H^{001}_{\mathrm{aniso,III}}$ for the etched sample could be associated with an inhomogeneous profile in D. Consequently, these adaptations of parameters for the etched sample impart an impression for the limitations of our model and the uncertainties also inherent to the other parameters, e.g., the thicknesses of the different layers. Nevertheless, except for these issues, the SWR spectrum of the etched sample can be explained by the model—with the same gradient G—as already applied successfully to

the as-grown sample, taking into account a reduction in the sample thickness by 51 nm upon etching.

VIII. PARTIALLY HYDROGENATED SAMPLE

An alternative approach to reduce the thickness of the ferromagnetic layer is postgrowth hydrogenation.[15,17] For increasing hydrogenation time we would expect the movement of a front into the sample separating a fully passivated paramagnetic layer from an unpassivated ferromagnetic one.[42] Therefore, short-time hydrogenation should lead to similar changes in the SWR spectrum as a reduction in sample thickness via etching. Indeed, upon short-time hydrogenation the spin-wave resonances are also shifted to smaller magnetic fields [Fig. 3(g)]. However, in contrast to the as-grown and the etched samples their intensities I_n exhibit an alternating behavior, which is indicative of a change in effective surface spin pinning. In our model we are able to reproduce this change in effective surface spin pinning via introducing an additional layer (I) with thickness $L_\mathrm{I}=10$ nm and anisotropy field $\mu_0 H^{001}_{\mathrm{aniso,I}}=-71$ mT [Fig. 3(i)]. Furthermore, in our simulation of the partially hydrogenated sample [Figs. 3(h) and 3(i)] we used $L_\mathrm{II}=67$ nm, $L_\mathrm{III}=6$ nm, $G=3.9$ mT/nm, $C=-472$ mT, $\mu_0 H^{001}_{\mathrm{aniso,III}}=-36$ mT, $D=5.9$ Tnm^2, $l=11.5$ nm, and $\mu_0 \Delta H_{\mathrm{pp}}=14$ mT. Here, the reduction in both L_II and C corresponds to a fully passivated region in the vicinity of the surface of thickness $L_0=22$ nm, as well as the presence of the additional layer (I) with reduced anisotropy field.

The nonmonotonic behavior of the intensities I_n can be qualitatively understood in terms of Fig. 3(i). For pinned spins, the additional half-wave oscillation in $\tilde{m}_n$ coming about for an increase in the mode index n by 1 has either only positive or only negative values. Thus, it alternately gives a positive or negative contribution to the total intensity integral (10). In contrast, for free spins the additional half wave always assumes both positive and negative values, leading to a continuous monotonic behavior. Note that in our simulation the pinning does not result from an *a priori* assumption of a change in surface spin pinning but from the introduction of the additional layer (I) with reduced $H_{\mathrm{un,I}}$, which serves as a "barrier" for $\tilde{m}_n(z)$ (*surface layer model*). The assumption of natural freedom—i.e., $\partial_z \tilde{m}=0$—at both surfaces of the ferromagnetic layer is still valid. Nevertheless, the change in surface spin pinning could alternatively be expressed also in the *surface anisotropy model*, taking into account the surface anisotropy field,[31]

$$\frac{2K_{\mathrm{surf}}}{M_{\mathrm{sat}}} = -L_\mathrm{I}[\mu_0 H_{\mathrm{un,I}}(z_\mathrm{I}) - \mu_0 H_{\mathrm{un,II}}(z_\mathrm{I})] = +4.0 \ \mathrm{T\,nm}. \tag{25}$$

The origin of a surface layer (I) is illustrated in Fig. 2. In our model we divide the hydrogenation profile into a fully passivated region (0), a partially hydrogenated region (I) corresponding to the tail in the hydrogenation profile, and an unpassivated region (II and III).[42] In the fully passivated region ferromagnetism will be suppressed completely, while in the unpassivated region magnetic properties will remain unchanged. The partially hydrogenated tail will lead to a region with rapidly changing hole concentration and thus rapidly changing uniaxial anisotropy field $H^{001}_{\mathrm{aniso}}(z)$. In our model we describe this region (I) in the most simple approximation via a steplike magnetic anisotropy profile with $H^{001}_{\mathrm{aniso,I}}(z_\mathrm{I}) \approx H^{001}_{\mathrm{aniso,II}}(z_\mathrm{I})/2 = C/2$. This approximation is possible since the large exchange stiffness in $Ga_{1-x}Mn_xAs$ averages out fluctuations in the anisotropy field on the length scale of the characteristic length $l=11.5$ nm. This is also obvious from the smoothness of the spin-wave profiles $\tilde{m}_n(z)$ in spite of the discontinuities in $H^{001}_{\mathrm{un}}(z)$ [Figs. 3(c), 3(f), and 3(i)]. Consequently, we can model the SWR spectrum of the sample hydrogenated for 2 h by the hydrogenation profile shown in Fig. 2(b) with a fully passivated region of thickness $L_0=22$ nm followed by a decline in H extending over $\approx L_1=10$ nm. This decline leads to a region of rapidly decreasing $H^{001}_{\mathrm{un}}(z)$ acting as a barrier for the spin-wave excitations. Therefore, short-time hydrogenation constitutes a simple method to efficiently manipulate the effective surface spin pinning.

IX. SWR FOR IN-PLANE MAGNETIC FIELDS

For $\vec{H}$ oriented along arbitrary directions the solution of Eq. (1) becomes quite challenging. On one hand the torques in two orthogonal directions in general are not equal and the precession of $\vec{M}$ about $\vec{H}_{\mathrm{eff}}$ therefore becomes elliptical. On the other hand the equilibrium orientation of magnetization $\vec{M}_{\mathrm{equ}}$ in general deviates from the orientation of $\vec{H}$ and thus *a priori* is unknown. This is even further complicated in the presence of an inhomogeneous $H^{001}_{\mathrm{aniso}}(z)$ which leads to an additional z dependence of $\vec{M}_{\mathrm{equ}}$. To simplify the evaluation of the in-plane SWR we will assume that $\vec{H}$ is oriented along a magnetic easy axis so that $\vec{M}_{\mathrm{equ}} \| \vec{H}$ is fulfilled, which is the case for $\vec{H} \| [010]$. Then a homogeneous film with a magnetic anisotropy given by the free-energy density (3) would exhibit a ferromagnetic resonance at the uniform resonance field,[6,31]

$$\mu_0 H^{\|}_{\mathrm{un,homogeneous}} = \frac{K^{001}_{\mathrm{eff}}}{M_{\mathrm{sat}}} - \frac{2K^{\|}_{c1}}{M_{\mathrm{sat}}} + \sqrt{\left(\frac{\omega}{\gamma}\right)^2 + \left(\frac{K^{001}_{\mathrm{eff}}}{M_{\mathrm{sat}}}\right)^2}. \tag{26}$$

To obtain a rough estimate for the gradient in $\mu_0 H^{\|}_{\mathrm{un}}$ of the $Ga_{0.95}Mn_{0.05}As$ layers under investigation, in the following we neglect the influence of the cubic anisotropy contributions in Eq. (26) and use the approximations

$$\mu_0 H^{\|}_{\mathrm{un}}(z) \approx \frac{1}{2}\mu_0 H^{001}_{\mathrm{aniso}}(z) + \sqrt{\left(\frac{\omega}{\gamma}\right)^2 + \left[\frac{1}{2}\mu_0 H^{001}_{\mathrm{aniso}}(z)\right]^2}$$
$$\approx \frac{\omega}{\gamma} - [G(z-z_\mathrm{I}) + C] \tag{27}$$

shown in Figs. 4(c), 4(f), and 4(i). There, $\mu_0 H^{\|}_{\mathrm{un}}(z)$ in region II is averaged by a linear gradient with the resulting effective G given in the figure. At this, we derived the values for $\mu_0 H^{\|}_{\mathrm{un}}(z_\mathrm{I})$ and $\mu_0 H^{\|}_{\mathrm{un}}(z_\mathrm{II})$ via insertion of $\mu_0 H^{001}_{\mathrm{aniso}}(z_\mathrm{I})$ and $\mu_0 H^{001}_{\mathrm{aniso}}(z_\mathrm{II})$ from the perpendicular resonance scenario dis-

cussed above [Figs. 3(c), 3(f), and 3(i)] into Eq. (27), respectively. Note that we thus relied on the same $\mu_0 H^{001}_{\text{aniso}}(z)$ profiles for the evaluation of $\mu_0 H^{\parallel}_{\text{un}}(z)$ as for $\mu_0 H^{001}_{\text{un}}(z)$ above. Using the circular precession approximation we thus can solve the spin-wave equation for $\vec{H}\|[010]$,

$$D\partial_z^2 \tilde{m}(z) + [-\mu_0 H + \mu_0 H^{\parallel}_{\text{un}}(z)]\tilde{m}(z) = 0, \qquad (28)$$

as already outlined above for the perpendicular orientation of the magnetic field. Figures 4(b), 4(e), and 4(h) again illustrate the graphical derivation of the sets of $\{l^2 k^2_{n,\text{II}}(z_{\text{I}}), l^2 k^2_{n,\text{II}}(z_{\text{II}})\}$ fulfilling both the boundary condition of natural freedom—represented by the set of curves A_n—and restriction (23) imposed by the gradient in $\mu_0 H^{\parallel}_{\text{un}}(z)$—represented by the straight diagonal lines. For these solutions the spin-wave excitations $\tilde{m}_n(z)$ are plotted at the positions of the corresponding resonance fields $\mu_0 H_{\text{res},n}$ in Figs. 4(c), 4(f), and 4(i). Finally, the dashed curves in Figs. 4(a), 4(d), and 4(g) represent the resulting SWR spectra with the intensities I_n calculated from Eq. (10) and $\mu_0 \Delta H_{\text{p.p.}} = 15$, 18, and 15 mT for the as-grown, the etched, and the partially hydrogenated samples, respectively. In comparison with experiment (full curves) we observe that for the etched and partially hydrogenated samples the simulated resonance fields are shifted to higher magnetic fields. This offset as well as the deviations in relative intensities we attribute to the influence of cubic anisotropy which has been neglected. However, the horizontally shifted straight vertical lines representing the resonance fields show that there is at least qualitative agreement with the observed SWR spacing. In this sense, we have shown that one and the same $\mu_0 H^{001}_{\text{aniso}}(z)$ is able to describe the SWR spectra observed for both $\vec{H}\|[001]$ and $\vec{H}\|[010]$.

Figures 5(a) and 5(b) compare the SWR spectra of the as-grown, the etched, and the partially hydrogenated samples for the external magnetic field oriented along the in-plane directions $[0\bar{1}1]$ and [010], respectively. In Eq. (3) the $[0\bar{1}1]$ axis corresponds to a magnetic easy orientation of the uniaxial and cubic anisotropy contributions perpendicular to the film plane, $-K^{001}_{\text{eff}} \alpha_z^2$ and $-\frac{1}{2} K^{\perp}_{c1} \alpha_z^4$, respectively, and to a magnetic hard orientation of the cubic anisotropy contribution within the film plane $-\frac{1}{2} K^{\parallel}_{c1}(\alpha_x^4 + \alpha_y^4)$. Therefore, especially the circular precession approximation is no longer justified. Nevertheless, we would like to briefly discuss the SWR spectra observed. The spectra of the as-grown sample exhibit a similar behavior as reported recently by Liu *et al.*[13] For $\vec{H}\|[010]$, i.e., along the easy axis, the spectrum already compared with the result of the SWR simulation in Fig. 4(a) features at least three spin-wave resonances with approximately constant level spacing, while for $\vec{H}\|[0\bar{1}1]$ a single resonance with high intensity accompanied by two much weaker resonances at higher magnetic field can be distinguished. The latter could be associated with surface modes.[13] Both upon etching and short-term hydrogenation the resonance for $\vec{H}\|[010]$ moves to smaller and the main resonance for $\vec{H}\|[0\bar{1}1]$ to larger magnetic fields. This is indicative of an *increase* in the in-plane cubic anisotropy $\mu_0 H^{\parallel}_{c1} = 2K^{\parallel}_{c1}/M_{\text{sat}}$ upon a reduction in the layer thickness. Note that this observation is consistent with Thevenard *et al.*,[20] who, in agreement with the results of mean-field calculations[4,43] for the typical range of carrier concentration, found that $\mu_0 H^{\parallel}_{c1}$ increases with decreasing hole density. Thus, the gradient in hole density present in our samples with the maximum carrier concentration at the sample surface not only leads to the gradient in $\mu_0 H^{001}_{\text{aniso}}$ already discussed above but also to a gradient in $\mu_0 H^{\parallel}_{c1}$. In contrast to $|\mu_0 H^{001}_{\text{aniso}}(z)|$, $|\mu_0 H^{\parallel}_{c1}(z)|$ exhibits its minimum at the sample surface and increases with depth z. While $\mu_0 H^{\parallel}_{c1}(z)$ has negligible influence on the SWR spectra for the external magnetic field oriented perpendicular to the film plane, it is expected to strongly influence the SWR spectra for the external magnetic field aligned within the film plane and thus can account for the deviations between the experiment and the SWR simulation in Fig. 4. However, a more sophisticated micromagnetic model—requiring neither $\vec{M}_{\text{equ}}\|\vec{H}$ nor the circular precession approximation to be fulfilled—is needed to fully account for the SWR observed for an arbitrary orientation of the magnetic field.

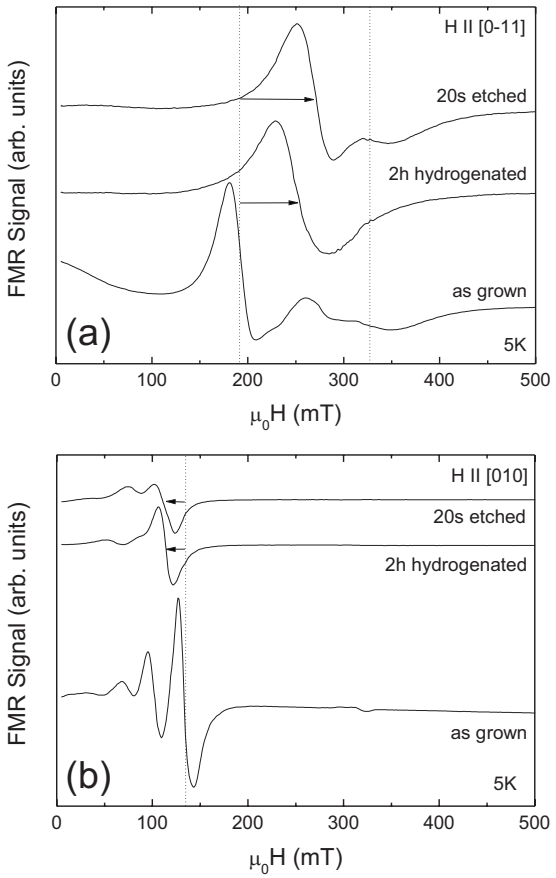

FIG. 5. (a) In-plane SWR spectra for $\vec{H}\|[0\bar{1}1]$ and (b) $\vec{H}\|[010]$. Both upon etching and hydrogenation the main resonance shifts to higher (lower) fields for $\vec{H}\|[0\bar{1}1]$ ($\vec{H}\|[010]$), indicating an increase in the in-plane cubic anisotropy field $\mu_0 H^{\parallel}_{c1}(z)$ from the surface to the film-substrate interface.

X. CONCLUSIONS

In summary, we have compared the SWR spectrum of an as-grown $Ga_{0.95}Mn_{0.05}As$ sample with those obtained after

etching and short-term hydrogenation. Our elaborate model quantitatively explains the SWR spectrum of the as-grown sample for the external magnetic field oriented perpendicular to the film plane and the changes upon sample treatment. Both the SWR spacings and the relative intensities can be reproduced via a linear gradient in the uniaxial magnetic anisotropy field in growth direction, which we attribute to the presence of a gradient in the hole concentration. In addition, upon short-time hydrogenation we observe a change in effective surface spin pinning which we attribute to the tail in the hydrogen-diffusion profile. This region of rapidly decreasing hole concentration leads to a region of a rapidly changing anisotropy profile acting as a barrier for the spin-wave excitations. Consequently, short-time hydrogenation constitutes an efficient method to manipulate the effective surface spin pinning. Our model also semiquantitatively explains the spacing of the SWR observed for the external magnetic field oriented along the magnetic easy axis within the film plane. The remaining deviations between our model and the experiment were attributed to the influence of cubic anisotropy, the discussion of which is beyond the scope of this paper.

ACKNOWLEDGMENT

The work was supported by Deutsche Forschungsgemeinschaft via SFB 631 (Walter Schottky Institut) and LI 988/4 (Universität Ulm).

*christoph.bihler@wsi.tum.de

[1] H. Ohno, Science **281**, 951 (1998).
[2] T. Jungwirth, J. Sinova, J. Mašek, J. Kučera, and A. H. MacDonald, Rev. Mod. Phys. **78**, 809 (2006).
[3] C. Bihler *et al.*, Phys. Rev. B **78**, 045203 (2008).
[4] T. Dietl, H. Ohno, and F. Matsukura, Phys. Rev. B **63**, 195205 (2001).
[5] D. M. Wang, Y. H. Ren, X. Liu, J. K. Furdyna, M. Grimsditch, and R. Merlin, Phys. Rev. B **75**, 233308 (2007).
[6] X. Liu and J. K. Furdyna, J. Phys.: Condens. Matter **18**, R245 (2006).
[7] C. Kittel, Phys. Rev. **110**, 1295 (1958).
[8] O. M. Fedorych, E. M. Hankiewicz, Z. Wilamowski, and J. Sadowski, Phys. Rev. B **66**, 045201 (2002).
[9] S. T. B. Goennenwein *et al.*, Appl. Phys. Lett. **82**, 730 (2003).
[10] Y. Sasaki, X. Liu, T. Wojtowicz, and J. K. Furdyna, J. Supercond. **16**, 143 (2003).
[11] T. G. Rappoport, P. Redlinski, X. Liu, G. Zarand, J. K. Furdyna, and B. Janko, Phys. Rev. B **69**, 125213 (2004).
[12] Y. Y. Zhou, Y.-J. Cho, Z. Ge, X. Liu, M. Dobrowolska, and J. K. Furdyna, IEEE Trans. Magn. **43**, 3019 (2007).
[13] X. Liu, Y. Y. Zhou, and J. K. Furdyna, Phys. Rev. B **75**, 195220 (2007).
[14] B. Hoekstra, R. P. van Stapele, and J. M. Robertson, J. Appl. Phys. **48**, 382 (1977).
[15] S. T. B. Goennenwein, T. A. Wassner, H. Huebl, M. S. Brandt, J. B. Philipp, M. Opel, R. Gross, A. Koeder, W. Schoch, and A. Waag, Phys. Rev. Lett. **92**, 227202 (2004).
[16] C. Bihler, M. Kraus, M. S. Brandt, S. T. B. Goennenwein, M. Opel, M. A. Scarpulla, R. Farshchi, D. M. Estrada, and O. Dubon, J. Appl. Phys. **104**, 013908 (2008).
[17] L. Thevenard, L. Largeau, O. Mauguin, A. Lemaître, and B. Theys, Appl. Phys. Lett. **87**, 182506 (2005).
[18] R. Farshchi, O. D. Dubon, D. J. Hwang, N. Misra, C. P. Grigoropoulos, and P. D. Ashby, Appl. Phys. Lett. **92**, 012517 (2008).
[19] K. Khazen, H. J. von Bardeleben, J. L. Cantin, L. Thevenard, L. Largeau, O. Mauguin, and A. Lemaître, Phys. Rev. B **77**, 165204 (2008).
[20] L. Thevenard, L. Largeau, O. Mauguin, A. Lemaître, K. Khazen, and H. J. von Bardeleben, Phys. Rev. B **75**, 195218 (2007).
[21] W. Limmer, M. Glunk, J. Daeubler, T. Hummel, W. Schoch, R. Sauer, C. Bihler, H. Huebl, M. S. Brandt, and S. T. B. Goennenwein, Phys. Rev. B **74**, 205205 (2006).
[22] V. Avrutin, D. Humienik, S. Frank, A. Koeder, W. Schoch, W. Limmer, R. Sauer, and A. Waag, J. Appl. Phys. **98**, 023909 (2005).
[23] L. Landau and E. Lifshitz, Phys. Z. Sowjetunion **8**, 153 (1935).
[24] T. L. Gilbert, IEEE Trans. Magn. **40**, 3443 (2004).
[25] J. Sinova, T. Jungwirth, X. Liu, Y. Sasaki, J. K. Furdyna, W. A. Atkinson, and A. H. MacDonald, Phys. Rev. B **69**, 085209 (2004).
[26] Note that the signs of the uniaxial parameters K_{eff}^{001} and K_{u}^{001} in Eq. (3) are defined opposite to earlier publications (Refs. 3, 44, and 45). According to Eq. (3) the growth direction corresponds to the magnetic easy axis of the uniaxial anisotropy contribution for a positive K_{eff}^{001}. The accompanied positive $\vec{H}_{\mathrm{aniso}}^{001}$ leads to an increase in precession frequency of $\vec{M}$ about $\vec{H}_{\mathrm{eff}}$ [cf. Eqs. (1) and (2)]. Taking into account microwave irradiation at constant frequency, the resonance condition (precession frequency equals microwave frequency) thus, is fulfilled at a decreased external magnetic field. Analogously, a negative K_{eff}^{001} leads to a magnetic hard axis along the growth direction and for $\vec{H}\|[001]$ to a shift of the ferromagnetic resonance to higher magnetic fields.
[27] A. Shen, H. Ohno, F. Matsukura, Y. Sugawara, N. Akiba, T. Kuroiwa, A. Oiwa, A. Endo, S. Katsumota, and Y. Iye, J. Cryst. Growth **175**, 1069 (1997).
[28] X. Liu, Y. Sasaki, and J. K. Furdyna, Phys. Rev. B **67**, 205204 (2003).
[29] J. Daeubler, S. Schwaiger, M. Glunk, M. Tabor, W. Schoch, R. Sauer, and W. Limmer, Physica E **40**, 1876 (2008).
[30] A. M. Portis, Appl. Phys. Lett. **2**, 69 (1963).
[31] B. Hoekstra, Ph.D. thesis, Philips Research Laboratories, 1978.
[32] H. Puszkarski, Prog. Surf. Sci. **9**, 191 (1979).
[33] A. R. Ferchmin, Phys. Lett. **1**, 281 (1962).
[34] H. Puszkarski, Solid State Commun. **22**, 563 (1977).
[35] G. T. Rado and J. R. Weertman, J. Phys. Chem. Solids **11**, 315 (1959).
[36] R. Soohoo, Phys. Rev. **131**, 594 (1963).
[37] E. Schlömann, J. Appl. Phys. **36**, 1193 (1965).
[38] A. Koeder *et al.*, Appl. Phys. Lett. **82**, 3278 (2003).
[39] W. Limmer *et al.*, Phys. Rev. B **71**, 205213 (2005).

[40] K. M. Yu, W. Walukiewicz, T. Wojtowicz, I. Kuryliszyn, X. Liu, Y. Sasaki, and J. K. Furdyna, Phys. Rev. B **65**, 201303(R) (2002).
[41] K. W. Edmonds *et al.*, Phys. Rev. Lett. **92**, 037201 (2004).
[42] C. P. Herrero, M. Stutzmann, A. Breitschwerdt, and P. V. Santos, Phys. Rev. B **41**, 1054 (1990).
[43] M. Abolfath, T. Jungwirth, J. Brum, and A. H. MacDonald, Phys. Rev. B **63**, 054418 (2001).
[44] C. Bihler, H. Huebl, M. S. Brandt, S. T. B. Goennenwein, M. Reinwald, U. Wurstbauer, M. Döppe, D. Weiss, and W. Wegscheider, Appl. Phys. Lett. **89**, 012507 (2006).
[45] C. Bihler, M. Kraus, H. Huebl, M. S. Brandt, S. T. B. Goennenwein, M. Opel, M. A. Scarpulla, P. R. Stone, R. Farshchi, and O. D. Dubon, Phys. Rev. B **75**, 214419 (2007).